

Passive Bistatic Imaging using Galileo Transmitter

R. Zuo, M. Antoniou, E. Plakidis, M. Cherniakov

School of Electronic, Electrical and Computer Engineering
University of Birmingham, Edgbaston, Birmingham, B15 2TT

Abstract

This paper presents research results on passive bistatic SAR. It discusses various system parameters, problems (e.g. parameter estimation, motion compensation), and signal processing algorithms (imaging, synchronization) required for bistatic SAR imaging. An experimental set-up for the verification of our system is described and an experimentally obtained image using Galileo satellite transmitter is analyzed.

Introduction

Synthetic aperture radar (SAR) is a type of radar used for imaging terrain. It utilises the relative motion between the radar antenna and a ground patch to generate high-resolution images. In a monostatic SAR the transmitter and receiver are on the same platform whereas in a bistatic SAR (BSAR) the transmitter and receiver are separated. Examples of BSAR include airborne systems where the transmitter and receiver are located on different aircraft [1], [2]; in a space-borne system the transmitter and receiver are based on two or more satellites [3]. In addition, there is another subclass of bistatic SAR known as space-surface bistatic synthetic aperture radar (SS-BSAR). SS-BSAR consists of a spaceborne transmitter and a receiver, mounted on or near the earth's surface. Its general topology is shown in Figure 1. The receiver could be airborne, mounted on a ground vehicle, onboard a ship, or even in a stationary position on the ground.

The University of Birmingham has been carrying out active research in the area of SS-BSAR since 2003. The main aim of this research is to experimentally demonstrate the feasibility and performance of airborne SS-BSAR, utilising Global Navigation Satellite System (GNSS) as transmitters of opportunity. This paper highlights and

briefly discusses various system parameters (resolution, power budget), problems (e.g. parameters estimation, motion compensation), and signal processing algorithms required for successfully obtaining an image. It also describes an experimental set-up with the receiver mounted on a ground moving vehicle and a Galileo satellite as the transmitter of opportunity, which was done in order to verify the developed algorithms. Finally, a first experimental image using our configuration is presented and analysed.

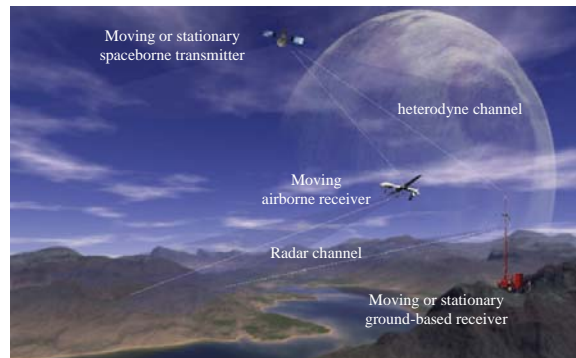


Figure 1: SS-BSAR topology

Ranging Signal

The Galileo satellite (GIOVE-A/B) was selected as the transmitter of opportunity for experimentation at the current stage, and its nominal E5 signal has been used for image formation. There are also navigation signals transmitted by other GNSS systems, for example GPS P/M-code and GLONASS

P-code which have similar signal structures and comparable spectral width to that of E5. It should be noted that although we are using a particular satellite/signal, the main principle of the radar system is generic and could be used with different GNSS transmitters. More details are given in [4] for using other GNSS as the transmitter for SS-BSAR.

$$x_{E5}(t) = [D_{E5al}(t) \cdot C_{E5al}(t) + jC_{E5aQ}(t)] \cdot [\text{sign}(\cos(2\pi f_s t)) + j\text{sign}(\sin(2\pi f_s t))] + [D_{E5bl}(t) \cdot C_{E5bl}(t) + jC_{E5bQ}(t)] \cdot [\text{sign}(\cos(2\pi f_s t)) - j\text{sign}(\sin(2\pi f_s t))] \quad (1)$$

Equation (1) above gives a simplified baseband E5 signal expression. $D_{E5al}(t)$ is the transmitted navigation message on E5a in-phase component, $C_{E5al}(t)$ is the spreading code of E5a in-phase component which will be actually applied as the ranging signal, and $\text{sign}(\cos(2\pi f_s t))$ is the binary sub-carrier splitting the mainlobe of the spreading code spectrum into two lobes (E5a and E5b) centred at the frequency of $\pm f_s$. Either E5a or E5b can be received individually to form an image, providing the minimal bandwidth of 10.23 MHz, hence 15 m slant range resolution in the quasi-monostatic case (highest one comparing Galileo E1, E5 and E6 signals) can be achieved. Alternatively, by receiving the full E5 signal, it's possible to combine and shift the E5a and E5b spectrum in such a way to achieve a spectral width of 20 MHz, therefore improving range resolution to ~ 8 m, since independent information is transmitted by them.

In terms of power budget for the E5 signal, with the minimum received power level, a 50 m^2 RCS target can be detected at a range of approximately 5 km considering 10-13 dB SNR detection threshold [5]. If the maximum signal power level (6 dB more than minimum power level on average due to the elevation) is considered, one can expect up to four times improvement in the maximum detection range.

Synchronisation

A fundamental problem associated with any non-cooperative bistatic radar is synchronisation between the transmitter and the receiver to allow for coherent signal processing. In spite of the fact that GNSS signals are optimised for remote synchronisation and the user has full knowledge of the transmitted signal, the synchronisation needs to be analysed from the radar application point of view. It can be seen from Figure 2 that the locally generated reference needs to be synchronised to the received heterodyne signal with delay, Doppler shift and phase variation in order to remove the main part of $f_s(u)$ from the radar channel signal, so that the azimuth signal history after range compression is mainly due to receiver-target motion $f_R(u)$, plus residual Doppler shift difference between $f_{RS}(u)$ and $f_s(u)$, which can be corrected or compensated at the later stages of image formation.

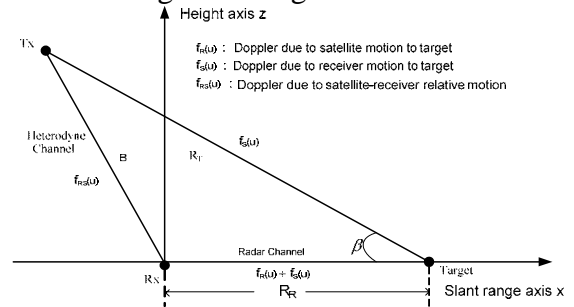


Figure 2: Instantaneous Bistatic Triangle

In our current experiments, since we consider E5b reception only, the signal received in the heterodyne channel, after quadrature demodulation, can be expressed as:

$$I_{E5b}(t) = D_{E5bl}(t - \tau_b) \cdot C_{E5bl}(t - \tau_b) \cdot \cos(\omega_s t + \phi(t)) + C_{E5bQ}(t - \tau_b) \cdot \sin(\omega_s t + \phi(t)) \\ Q_{E5b}(t) = D_{E5bl}(t - \tau_b) \cdot C_{E5bl}(t - \tau_b) \cdot \sin(\omega_s t + \phi(t)) - C_{E5bQ}(t - \tau_b) \cdot \cos(\omega_s t + \phi(t)) \quad (2)$$

where $I_{E5b}(t)$ and $Q_{E5b}(t)$ are the in-phase and quadrature components at the demodulator output, $\phi(t)$ represents unknown phase variation, τ_b and ω_s are the delay and Doppler shift suffered by the

signal during propagation from the satellite to the receiver.

Figure 3 below shows a simplified block diagram of the synchronisation algorithm applied to the heterodyne signal. It consists of acquisition, secondary code extraction, and three main tracking blocks. From Equation (2) it can be seen that, unlike E5b-I, there is no need for navigation message decoding using E5b-Q. With all the tracked parameters, the locally generated E5b-Q can then be modulated and used as the reference signal for range compression. The main tracking algorithm is widely used in software GNSS receivers and is comprehensively discussed in [6]. Figure 4&5 below show the tracking output from experimental data. Due to the noise in the heterodyne channel, tracked Doppler shift varies with 10-20 Hz range (Figure 5). A linear least mean square (LMS) process is applied to it and its output is used as tracked Doppler shift from the heterodyne signal.

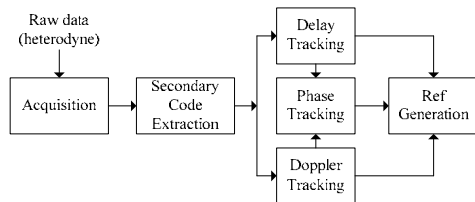


Figure 3: Synchronisation Block Diagram

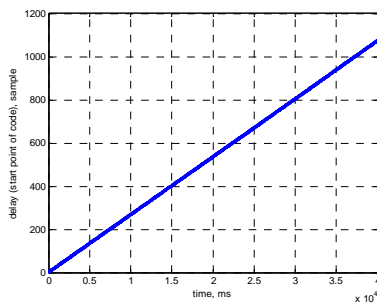


Figure 4: Tracked Fine Delay

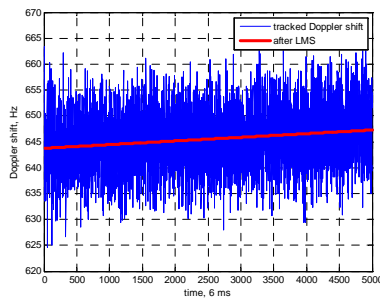


Figure 5: Tracked Fine Doppler Shift

SS-BSAR Imaging

Our research has been focused on the derivation of a generalised image formation algorithm designed specifically for SS-BSAR operating in Stripmap mode. In this section, a conceptual description of the algorithm will be provided. A specific configuration is assumed, where the transmitter is a GNSS satellite and the receiver is airborne. A full description of the algorithm can be found in [7], along with detailed descriptions of algorithms designed for other SS-BSAR configurations.

A block diagram of the generalised SS-BSAR image formation algorithm with integrated motion compensation (MoComp) to account for receiver motion errors is shown in Figure 6.

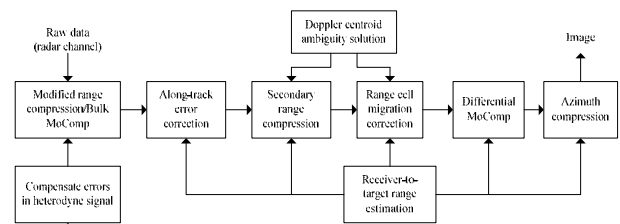


Figure 6: Image Formation with Motion Compensation

The first step in the algorithm is to equalize the range and Doppler histories of targets residing at the same range from the receiver. This is achieved by correlating the received data with the locally (computer) generated reference signal obtained at the synchronization output. This signal is equivalent to the direct signal received from the satellite. Prior to this step, the algorithm assumes that motion errors in the direct signal have been compensated. The modified range compression is performed in the range-frequency, azimuth-time domain. At the output of this step, the range and Doppler histories of targets at the same range, but different cross-range become very similar for a wide range of possible geometries. Since the transmitter-to-target and receiver-to-target ranges can normally be approximated using second-order Taylor

series expansions in SS-BSAR, it is also possible to derive signal expressions in the frequency domain. Therefore, use of a modification of the Range-Doppler algorithm is a convenient method to form the image of an observation area. A secondary range compression (SRC) is performed to compensate for the cross-coupling between the range and azimuth frequencies. Before this operation is executed, the Doppler ambiguity is resolved (that is because the target azimuth signature could contain a large Doppler centroid outside the range of sampled azimuth frequencies). Range cell migration (RCM) is corrected in the range-time, azimuth-frequency (or range, Doppler) domain, after RCM components due to the receiver motion and residual RCM after the modified range compression are calculated. For this operation, it is proposed to estimate the receiver-to-target range from the range sum (the difference between the total range history and the transmitter-to-receiver range history) in order to identify the individual RCM components mentioned above. Finally, azimuth compression is performed in the range, Doppler domain. Finally, it is noted that the structure of MoComp is similar to that employed by conventional airborne monostatic SAR systems.

Experimentation Set-up

With the experience gained from previous SS-BSAR imaging experiments using GLONASS on a controlled track carriage system [4], an experimental trial using Galileo satellite has been proposed with the receiver mounted on a ground moving vehicle to imitate the motion of a real aircraft. Figure 7 shows the selected experiment site for data collection, which is located at Cleehill, West Midlands.

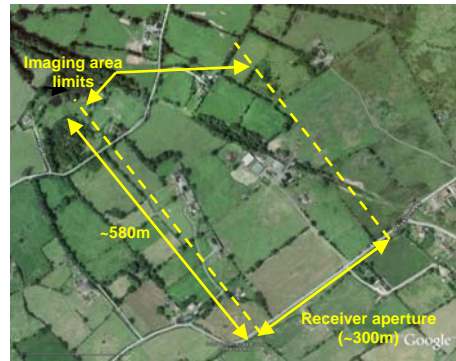


Figure 7: Experiment Site

The experimental parameters have then been designed accordingly. With up to 300 m fairly straight path available and $\sim 5^\circ$ radar antenna looking angle, the main parameters are calculated and shown in Table 1.

Table 1: Experimental Parameters

E5 signal power density (W/m^2)	3×10^{-14}
Central Frequency (MHz)	1207.14
Signal Bandwidth (MHz)	10.23
Aperture length (m)	300
Transmitter velocity (m/s)	2500
Receiver velocity (m/s)	7-10
Integration time (s)	30-40
Receiver-target ground range (m)	100-1000

Figure 8 below displays the hardware used during the vehicle trial. Three antennas were mounted on the roof of the vehicle, one directional radar channel antenna (16 dB gain with 30° beamwidth), and two omni-directional antennas for heterodyne (direct signal) channel and GPS receiver (positioning) respectively.



Figure 8: Experimental Vehicle Set-up

Parameter Estimation & Motion Compensation

Besides the parameters tracked from the signal itself (Figure 5), there are also steps requiring the knowledge of information such as transmitter trajectory, receiver position/velocity, target Doppler centroid etc. Estimation of these parameters is not only vital for extracting motion errors and compensating them, but also important for calculating the nominal target range/Doppler histories used for Range Cell Migration Correction (RCMC) and azimuth filter generation.

Since the Galileo transmitter is a satellite, its trajectory is normally a stable and deterministic path and its geographic coordinates at a specific time can be estimated using real time ephemeris or other sources of satellite orbit information. The receiver position/velocity history of our experiment is derived from stored GPS observation data combined with International GNSS Service (IGS) precise orbit information, to achieve accuracy within centimeters level. Figures 8 and 9 below show the results of receiver position and velocity estimations. It is clearly visible that the receiver motion error can be up to about 1 meter in any direction, much larger than the wavelength.

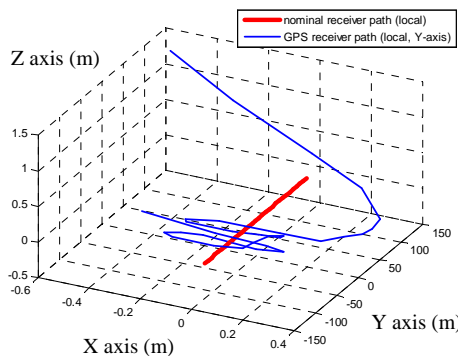


Figure 8: Receiver Trajectory with Motion Errors

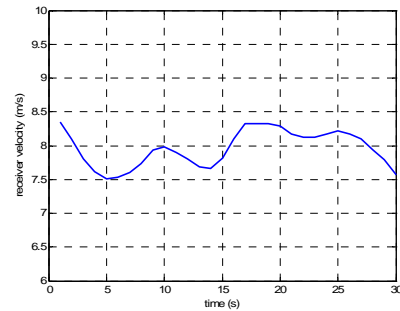


Figure 9: Receiver Velocity History

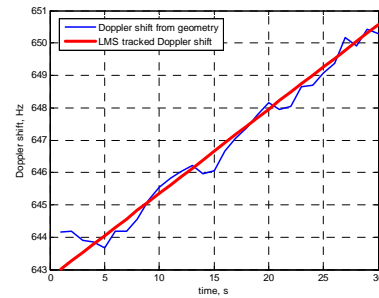


Figure 10: Doppler shift history in heterodyne channel

With high precision estimation of both satellite and receiver's trajectory and velocity histories, Doppler shift/phase variation in the heterodyne channel can also be calculated from transmitter-receiver geometry. Figure 10 above compares Doppler shift between the tracked one from synchronisation and the one from parameter estimation. The good match at Doppler bandwidth between two results validates the synchronisation algorithm; moreover with the minor difference between two Doppler shift estimations, appropriate motion/phase compensation can be applied to the heterodyne channel for any undesired receiver motion effects.

First Experimental Image

A SAR intensity image, superimposed on a satellite photograph of our target area is shown in Figure 11.

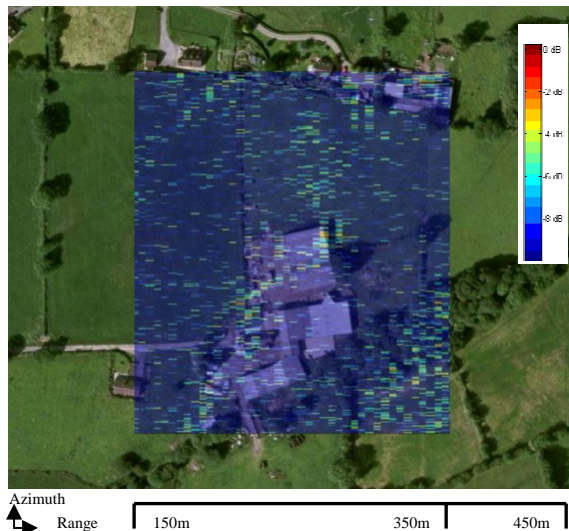


Figure 11: Experimental Bistatic SAR Image

As can be seen in Figure 11, the dominant target is an extended structure towards the middle of the scene (at a range of approximately 250m). The building orientation resembles an L-shape, and should therefore be readily identifiable in the radar image. Observation of Figure 11 shows that this building (and its L-pattern) has been detected. Moreover, buildings on the upper side of the imaging area are visible. The area surrounding these buildings is grassland, and therefore its intensity is lower. Parts of the forested area towards the site of the building can also be seen.

With this image some signal processing blocks have been skipped in our image formation algorithm. In particular, secondary range compression was not implemented. Furthermore, in order to avoid range/azimuth coupling (due to the large Doppler centroid introduced by the motion of the satellite), only a bulk range migration correction was performed, correcting only the range migration of a target at the imaging scene centre. For these reasons we only concentrated on a narrow imaging area around the L-shaped building. Another factor affecting image quality is currently the output of our synchronisation algorithm. The tracked Doppler of the direct transmitter-receiver signal contains a part of receiver motion errors, but this

amount is unknown (due to the fact that a least-mean square algorithm is applied to get an average estimate). Since this tracked Doppler is mixed with the transmitter-target-receiver Doppler, the mixed signal (and hence the final image product) contains motion errors too.

We believe that the above factors are responsible for limiting the quality of our image in terms of contrast and proper focus. Even so, it appears that we have obtained a first intensity image which corresponds to the reflectivity of the inspected terrain.

Conclusions

This paper gave an overview of the research carried out by the University of Birmingham in the area of SS-BSAR, utilising microwave emissions from GNSS transmitters as the ranging signal. Galileo satellites were used for experimentation. Some of the practical problems (such as synchronisation, parameter estimation) were also briefly discussed. An imaging algorithm for SS-BSAR was briefly discussed and experimentally tested. Using the moving vehicle, a first bistatic image was obtained. The next stage of our work will concentrate on improving the quality of this image by compensating for errors explained throughout the paper. The final stage of research is to conduct the final airborne trials.

Acknowledgements

The work reported in this paper was funded by the Electro-magnetic Remote Sensing (EMRS) Defence Technology Centre, established by the UK Ministry of Defence and run by a consortium of SELEX Galileo, Thales UK and Roke Manor Research.

References

1. Dubois-Fernandez P. et al., "ONERA-DLR bistatic SAR campaign: planning, data acquisition, and first analysis of bistatic scattering behaviour of natural and urban targets", *IEE Proceedings in Radar, Sonar and Navigation*, 2006, 153, pp.214- 223.
2. Walterscheid I. et al., "Bistatic SAR processing and experiments", *IEEE*

- Transactions on Geoscience and Remote Sensing*, 2006, 153, pp.2710-2717.
3. Moccia A. et al., "Spaced-borne bistatic synthetic aperture radar for remote sensing applications", *International Journal of Remote Sensing*, 2000, 21(18), pp.3395-3414.
 4. Cherniakov M., Saini R., Zuo R., Antoniou M., "Space-Surface bistatic synthetic aperture radar with global navigation satellite system transmitter of opportunity – experimental results", *IET Radar, Sonar and Navigation (RSN)*, Vol. 1, issue 6, pp. 447-458, December, 2007.
 5. Cherniakov M., Saini R., Antoniou M., Zuo R., Plakidis E., "Experiences gained during the development of a passive BSAR with GNSS transmitters of opportunity", *International Journal of Navigation and Observation*, Vol. 2008.
 6. Saini R., Zuo R., Cherniakov M., "Problem of Signal Synchronisation in SS-BSAR based on Global Navigation Satellite Emissions - Experimental Results", *IET Radar, Sonar and Navigation (RSN)*, accepted and under review.
 7. Antoniou M., Cherniakov M., Hu C., "Space-Surface BSAR image formation algorithms", to appear in *IEEE Transactions on Geoscience and Remote Sensing*, Vol. 47, issue 4, 2009.